Available online at www.sciencedirect.com
ScienceDirect
Ceramics International 36 (2010) 1109–1115
CERAMICS INTERNATIONAL
www.elsevier.com/locate/ceramint

Effect of dopant (Al, Nb, Bi, La) on varistor properties of $ZnO–V_2O_5–MnO_2–Co_3O_4–Dy_2O_3$ ceramics

Choon-W. Nahm *

Semiconductor Ceramics Lab., Department of Electrical Engineering, Dongeui University, Busan 614-714, Republic of Korea

Received 20 September 2009; received in revised form 15 October 2009; accepted 25 November 2009
Available online 4 January 2010

Abstract

The electrical, dielectric properties, and aging behavior of $ZnO–V_2O_5–MnO_2–Co_3O_4–Dy_2O_3$ (ZVMCD) ceramics were investigated with different dopants (Al, Nb, Bi, La). The phase formed for all the samples consisted of ZnO grain as a main phase, and $Zn_3(VO_4)_2$, ZnV_2O_4, and $DyVO_4$ as the secondary phases. On one hand, Nb and Bi dopants enhanced the nonlinear coefficient whereas Al and La dopants decreased it. On the other hand, Nb and Al improved the stability against aging stress. The Nb-doped ZVMCD ceramics exhibited the best nonlinear properties ($\alpha = 36$) and the highest stability: $\%\Delta E_B = -0.4\%$, $\%\Delta\alpha = -20\%$, $\%\Delta\varepsilon'_{APP} = -1.3\%$, and $\%\Delta\tan\delta = +13\%$ for DC accelerated aging stress of 0.85 E_B/85 °C/24 h.

Keywords: C. Nonlinear electrical properties; Stability; D. ZnO; V_2O_5; E. Varistor

1. Introduction

Impurity doped-ZnO ceramics exhibit the nonlinear electrical behavior, which is very similar to a back-to-back zener diode. The sintering process gives rise to a microstructure, which consists of semiconducting n-type ZnO grains surrounded by very thin insulating intergranular layers. Each ZnO grain acts as if it has a semiconductor junction at the grain boundary. Since nonlinear electrical behavior occurs at each boundary, the impurity doped ZnO ceramics can be considered as a multi-junction device composed of many series and parallel connection of grain boundaries. The grain size distribution plays a major role in electrical behavior. Electrically, ZnO varistors exhibit highly nonlinear voltage–current (U–I) properties expressed by the relation $I = KU^{\alpha}$, where I is the current, U is the voltage, K is a constant, α is the nonlinear coefficient, which characterizes the nonlinear properties of the varistors [1,2].

ZnO ceramics cannot exhibit a varistor behavior without adding heavy elements with large ionic radii such as Bi, Pr, Ba, etc. Commercial $ZnO–Bi_2O_3$-based ceramics and $ZnO–Pr_6O_{11}$-based ceramics cannot be co-fired with a silver inner-electrode (m.p. 961 °C) in mutilayered chip components because of the relatively high sintering temperature above 1000 °C [3,4]. Therefore, new varistor ceramics are required in order to use a silver inner-electrode. Among the various ceramics, one candidate is the $ZnO–V_2O_5$ ceramics [5–14]. This system can be sintered at a relatively low temperature in the vicinity of about 900 °C. This is very important for multilayer chip component applications, because it can be co-sintered with a silver inner-electrode without using expensive palladium or platinum metals.

A study on $ZnO–V_2O_5$-based ceramics is initial step yet in terms of materials composition and sintering process. To develop useful $ZnO–V_2O_5$-based ceramics, it is very important to investigate the effects of dopants on varistor properties. Until now, $ZnO–V_2O_5$-based ceramics have been reported for a ternary system containing MnO_2 [10–14]. $ZnO–V_2O_5–MnO_2$ ceramics is reported to exhibit good nonlinear properties (nonlinear coefficient measured between 1.0 mA cm^{-2} and 10 mA cm^{-2}, $\alpha \approx 27$) in previous research [13,14]. The Co and Dy are added to $ZnO–Bi_2O_3$-based ceramics or $ZnO–Pr_6O_{11}$-based ceramics to improve the varistor properties. In this report, the effect of dopant (Al, Nb, Bi, La) on varistor properties and aging behavior of $ZnO–V_2O_5–MnO_2–Co_3O_4–Dy_2O_3$ (ZVMCD) ceramics was examined.

* Tel.: +82 51 890 1669; fax: +82 51 890 1664.
E-mail address: cwnahm@deu.ac.kr.

0272-8842/$36.00
doi:10.1016/j.ceramint.2009.12.002

2. Experimental procedure

2.1. Sample preparation

Reagent-grade raw materials were prepared in the proportions of $(96.9 - x)$ mol% ZnO, 0.5 mol% V_2O_5, 2.0 mol% MnO_2, 0.5 mol% Co_3O_4, 0.1 mol% Dy_2O_3 (ZVMCD) and independent samples of 0.005 mol% Al_2O_3, 0.1 mol% Nb_2O_5, 0.1 mol% Bi_2O_3, and 0.1 mol% La_2O_3. Raw materials were mixed by ball milling with zirconia balls and acetone in a polypropylene bottle for 24 h. The mixture was dried at 120 °C for 12 h. The dried mixture was mixed into a container with acetone and 0.8 wt% polyvinyl butyral (PVB) binder of powder weight. After drying at 120 °C for 24 h, the mixture was granulated by sieving through a 100-mesh (150 μm) screen to produce starting powder. The powder was uniaxially pressed into discs of 10 mm in diameter and 1.3 mm in thickness at a pressure of 100 MPa. The discs were sintered at 900 °C in air for 3 h and furnace cooled to room temperature. The final samples were about 8 mm in diameter and 1.0 mm in thickness. Silver paste was coated on both faces of the samples and the ohmic contacts were formed by heating it at 600 °C for 10 min. The electrodes were 5 mm in diameter.

2.2. Microstructure analysis

Both surfaces of the samples were lapped and ground with SiC paper and polished with 0.3 μm-Al_2O_3 powder to a mirror-like surface. The polished samples were chemically etched into $1HClO_4$:$1000H_2O$ for 25 s at 25 °C. The surface of the samples was metallized with a thin coating of Au to reduce charging effects and to improve the resolution of the image. The microstructure was examined by a scanning electron microscope (SEM, Hitachi S2400). The average grain size (d) was determined by the lineal intercept method such as the expression, $d = 1.56L/MN$ [15], where L is the random line length on the micrograph, M is the magnification of the micrograph, and N is the number of the grain boundaries intercepted by the lines. The crystalline phases were identified by an X-ray diffractometry (XRD, X'pert-PRO MPD, Netherlands) with Ni filtered CuK_α radiation. The sintered density (ρ) of the ceramics was measured by the Archimedes method.

2.3. Electrical measurement

The electric field–current density (E–J) characteristics were measured using a high voltage source unit (Keithley 237). The breakdown field (E_B) was measured at 1.0 mA cm^{-2} and the leakage current density (J_L) was measured at 0.8 E_B. In addition, the nonlinear coefficient (α) is defined by the empirical law, $J = K \cdot E^{\alpha}$, where J is the current density, E is the applied electric field, and K is a constant. The α was determined in the current density range 1.0–10 mA cm^{-2}, where $\alpha = 1/(\log E_2 - \log E_1)$, and E_1 and E_2 are the electric fields corresponding to 1.0 mA cm^2 and 10 mA cm^2, respectively.

2.4. Dielectric measurement

The dielectric characteristics, such as the apparent dielectric constant (ε'_{APP}) and dissipation factor (tan δ) were measured in the range of 100 Hz to 2 MHz using a RLC meter (QuadTech 7600).

2.5. DC accelerated aging characteristic measurement

The DC accelerated aging test was performed for stress state of 0.85 E_B/85 °C/24 h. Simultaneously, the leakage current was monitored at intervals of 1 min during stressing using a high voltage source unit (Keithley 237). The degradation rate coefficient (K_T) was calculated by the expression $I_L = I_{Lo} + K_T t^{1/2}$ [16], where I_L is the leakage current at stress time (t) and I_{Lo} is I_L at $t = 0$. After applying the respective stresses, the E–J characteristics were measured at room temperature.

3. Results and discussion

Fig. 1 shows SEM micrographs of surface of the samples for different dopants. The grain structure is relatively homogeneously distributed throughout the entire samples, compared with ternary ZnO–V_2O_5–MnO_2 ceramics [10]. The average grain size (d) decreased in order of ZVMCD-Nb (7.5 μm) > ZVMCD-Bi (5.0 μm) > ZVMCD (4.6 μm) > ZVMCD-La (4.6 μm) > ZVMCD-Al (4.2 μm). It was found that the Nb and Bi dopants improved the grain growth, whereas the Al dopant inhibited it. The sintered density (ρ) was 5.56 g cm^{-3}, in the ZVMCD, ZVMCD-Al, and ZVMCD-Nb, whereas it was 5.44 g cm^{-3} in ZVMCD-Bi. It is presumed that the low sintered density of the ZVMCD-Bi is attributed to the larger ionic radius of Bi than Zn ion. The detailed density and average grain size of the samples are indicated in Table 1. The XRD patterns of the samples are shown in Fig. 2. All the samples revealed the presence of the secondary phase such as $Zn_3(VO_4)_2$, ZnV_2O_4, and $DyVO_4$. The $Zn_3(VO_4)_2$ is formed when the ZnO–V_2O_5-based ceramics are sintered at high temperatures and that acts as a liquid-phase sintering aid [5]. Furthermore, it seems that the $DyVO_4$ phase acts as an enhancer for the grain growth of ZnO [17].

Table 1 reports the main electrical characteristics of the samples for different dopants. The breakdown field (E_B) decreased in order of ZVMCD (7013 V cm^{-1}) > ZVMCD-La (4772 V cm^{-1}) > ZVMCD-Bi (4367 V cm^{-1}) > ZVMCD-Nb (3355 V cm^{-1}) > ZVMCD-Al (2514 V cm^{-1}). The decrease of E_B can be explained by both the increase in the number of grain boundaries owing to the increase in the average ZnO grain size and the decrease of breakdown voltage per grain boundaries ($_{gb}$), as expressed by the following equation [1]; $E_B = {}_{gb}/d$, where d is the grain size and $_{gb}$ stands for the breakdown voltage per grain boundaries. It should be noted that the ZVMCD-Al exhibited the lowest E_B although the grain size is the smallest. The addition of Nb and Bi dopants enhanced the nonlinear coefficient, whereas the Al and La dopants decreased it. It should be noted that the ZVMCD-Nb exhibited the highest value (36) among ZnO–V_2O_5-based ceramics reported up to

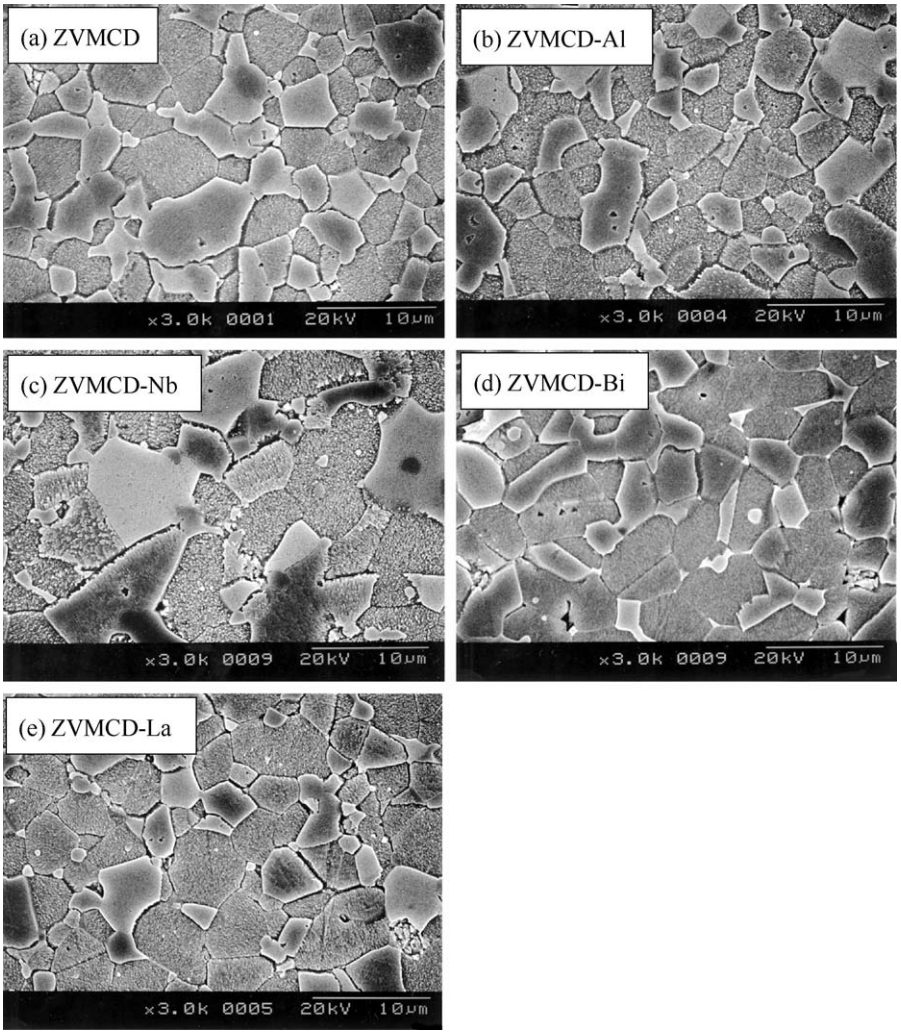

Fig. 1. SEM micrographs of the samples for different dopants.

now. These are a higher value than that of $ZnO–V_2O_5$-based multi-component ceramics prepared by microwave sintering process [7]. The high barrier caused by the electronic states at active grain boundary will give rise to a large α. In general, the leakage current (I_L) shows an opposite relation to the nonlinear coefficient (α). On the whole, the I_L value is much higher than the expected value in the light of α value. Presumably, a high leakage current of these samples seems to be due to the recombination of electron and hole rather than thermionic emission over barrier at the grain boundary.

Fig. 3 shows the apparent dielectric constant (ε'_{APP}) and dissipation factor ($\tan\delta$) of the samples for different dopants. With increasing frequency for all varistors, the ε'_{APP} decreased with a relatively sharp dispersive drop in the vicinity of 100 Hz which is closely associated with the interfacial polarization of dielectrics. The ε'_{APP} in the frequency above 1 kHz increased in order of ZVMCD-Al > ZVMCD-Nb > ZVMCD-Bi > ZVMCD-La > ZVMCD. This is directly related to d/t ratio, as can be seen in the following equation, $\varepsilon'_{APP} = \varepsilon_g(d/t)$, where ε_g is the dielectric constant of ZnO (8.5), d is the average grain size, and t is the depletion layer width of the both sides at the grain boundaries. On the other hand, the $\tan\delta$ decreased until the vicinity of 20 kHz with increasing frequency, which exhibits a second dispersion peak in the

Table 1
Microstructure, *E–J*, and dielectric characteristic parameters of the samples for different dopants.

Sample	d (μm)	ρ (g cm^{-3})	E_B (V cm^{-1})	V_{gb} (V gb^{-1})	α	J_L (μA cm^{-2})	ε'_{APP} (1 kHz)	$\tan\delta$ (1 kHz)
ZVMCD	4.6	5.56	7013	3.3	32	90	385	0.23
ZVMCD-Al	4.2	5.56	2514	1.1	17	334	1555	0.26
ZVMCD-Nb	7.5	5.55	3355	2.5	36	85	775	0.31
ZVMCD-Bi	5.0	5.44	4367	2.2	35	42	621	0.15
ZVMCD-La	4.6	5.50	4772	2.2	12	403	631	0.5

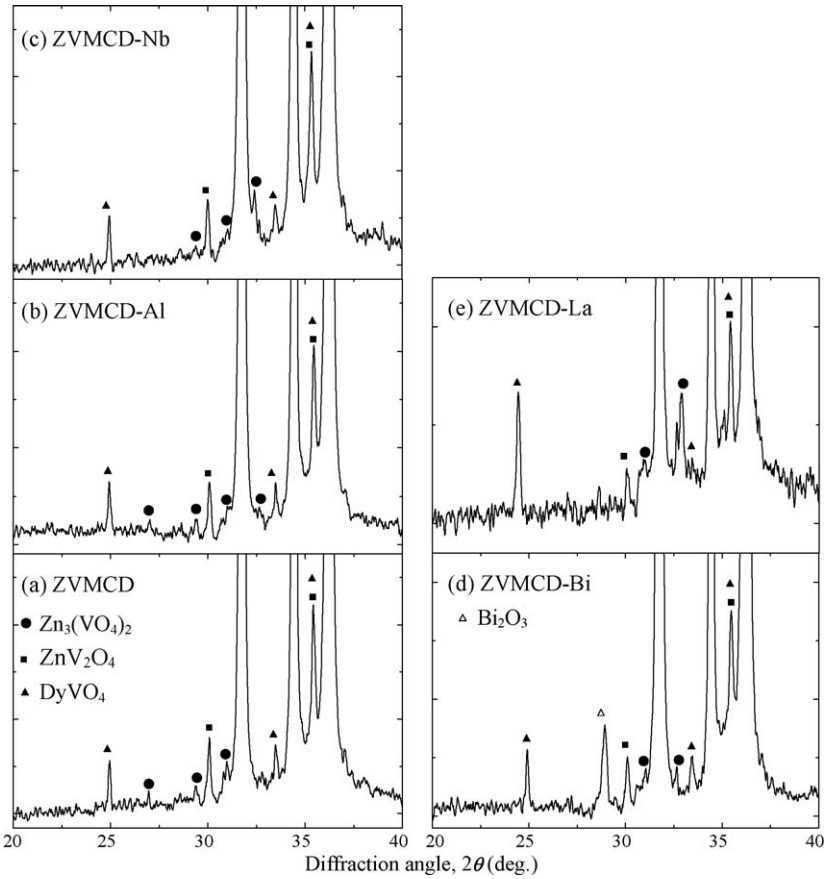

Fig. 2. XRD patterns of the samples for different dopants.

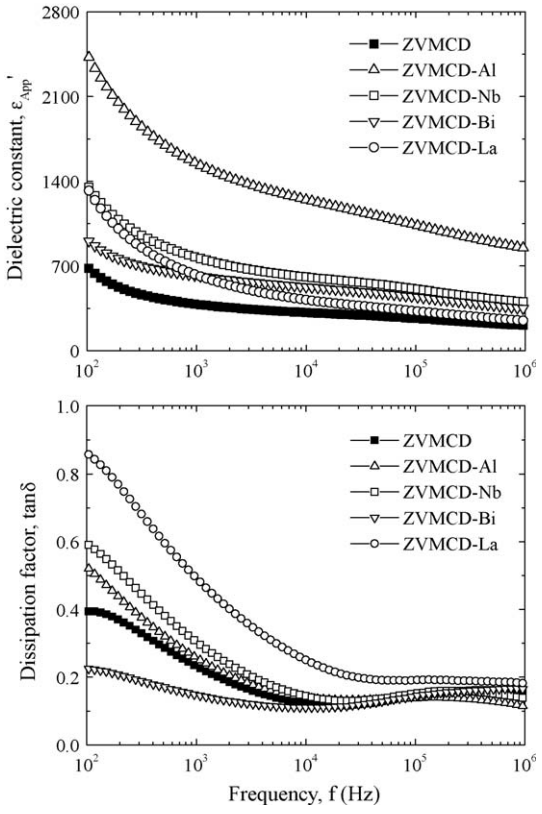

Fig. 3. Dielectric characteristics of samples for different dopants.

vicinity of 300 kHz, and thereafter again decreased. The detailed dielectric characteristic parameters at 1 kHz are summarized in Table 1.

Fig. 4 shows the variation of leakage current during DC accelerated aging stress of the samples for different dopants. It can be seen that the dopants have a significant effect on aging behavior. All the samples except for the ZVMCD-Al and ZVMCD-Nb exhibited thermal run-away under specified DC accelerated aging stress of 0.85 E_B/85 °C/24 h. The La and Bi

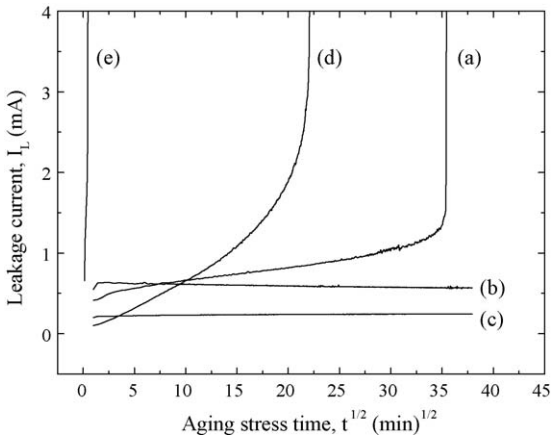

Fig. 4. Leakage current during accelerated aging stress of samples for different dopants: (a) ZVMCD, (b) ZVMCD-Al, (c) ZVMCD-Nb, (d) ZVMCD-Bi, and (e) ZVMCD-La.

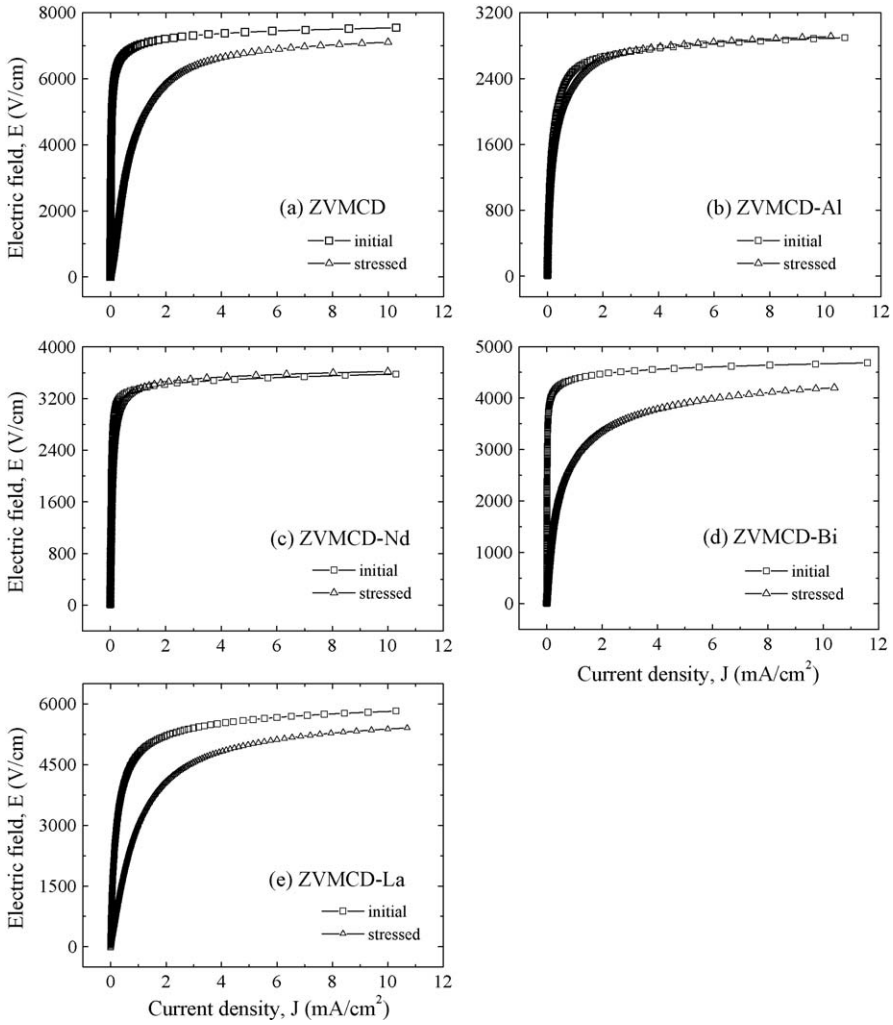

Fig. 5. *E–J* characteristics after applying stress of samples for different dopants.

dopants impaired the stability against accelerated aging stress. In particular, the Bi dopant improved the nonlinear electrical properties, whereas it resulted in a severe problem in stability. On the contrary, the ZVMCD-Al and ZVMCD-Nb were found to exhibit a good stability without thermal run-away during specified stress time period. The stability for nonlinear properties of the samples can be estimated by the degradation rate coefficient (K_T), indicating the degree of aging from the slope of the I_L–$t^{1/2}$ curve. The lower the K_T, the higher the stability. The ZVMCD-Al exhibited low value: -13 nA h$^{-1/2}$, whereas ZVMCD-Nb exhibited extremely low value: +4 nA h$^{-1/2}$.

Fig. 5 compares the variation of *E–J* characteristics after applying the stress with initial *E–J* characteristics for the respective samples. It can be seen that the variation of *E–J* curves after applying the stress is strongly affected by the dopants. The ZVMCD, ZVMCD-Bi, and ZVMCD-La exhibited very large variation of *E–J* curves in the entire range of electric field after applying the stress. However, the ZVMCD-Al and ZVMCD-Nb exhibited small variation in *E–J* curves after applying the stress, in particular, in the ZVMCD-Nb case.

Fig. 6 compares the variation of E_B after applying the stress with initial E_B for the respective samples. The ZVMCD, ZVMCD-Bi, and ZVMCD-La, which revealed a thermal run-away, exhibited a high variation, reaching approximately -35% in breakdown field ($\%\Delta E_B$). The ZVMCD-Al exhibited, high stable E_B characteristics reaching -6% in $\%\Delta E_B$. In particular, the ZVMCD-Nb exhibited the highest stable E_B

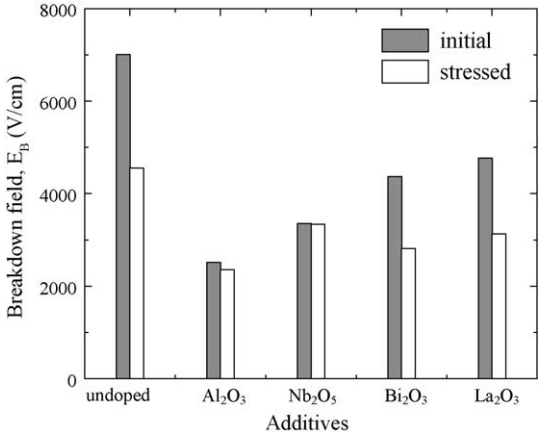

Fig. 6. Breakdown field before and after applying stress of samples for different dopants.

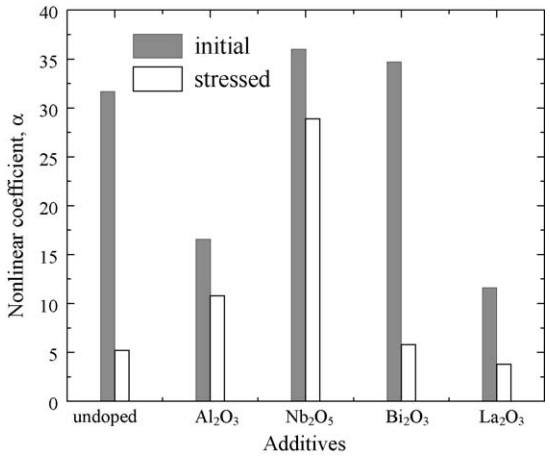

Fig. 7. Nonlinear coefficient before and after applying stress of samples for different dopants.

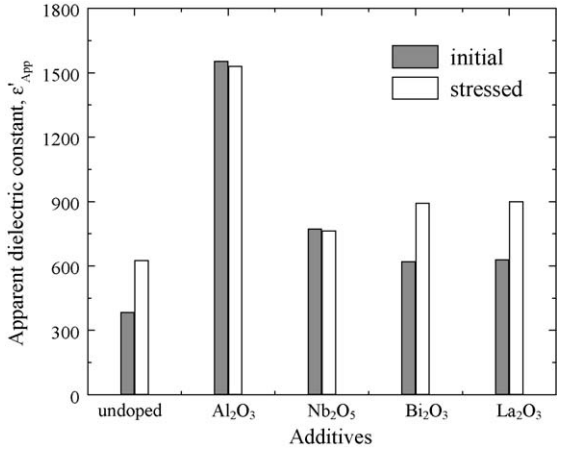

Fig. 8. Dielectric constant before and after applying stress of samples for different dopants.

characteristics showing $\%\Delta E_B = -0.4\%$ so there is almost no variation before and after applying the stress. Fig. 7 compares the variation of α after applying the stress with initial α for the respective samples. The ZVMCD, ZVMCD-Bi, and ZVMCD-La, which revealed a thermal run-away, exhibited extremely bad nonlinear properties by decreasing to inside and outside $\alpha = 5$ after applying the stress. The ZVMCD-Nb exhibited the

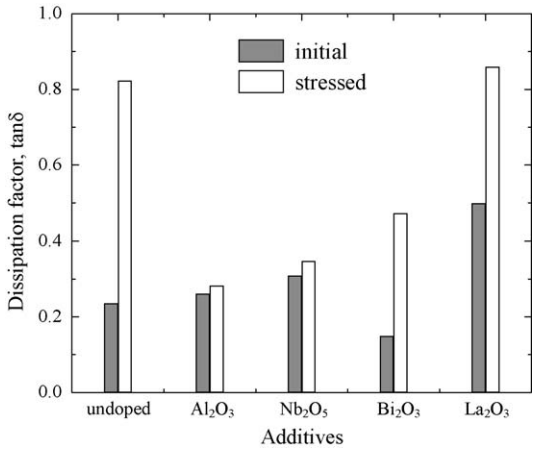

Fig. 9. Dissipation factor before and after applying stress of samples for different dopants.

highest stable α characteristics showing $\%\Delta\alpha = -20\%$. On the other hand, the ε'_{APP} and tan δ before and after applying the stress is shown in Figs. 8 and 9, respectively. The ZVMCD, ZVMCD-Bi, and ZVMCD-La, which revealed a thermal run-away, exhibited a high variation for ε'_{APP} and tan δ. However, the ZVMCD-Al and ZVMCD-Nb exhibited very small variation. In particular, the $\%\Delta\varepsilon'_{APP}$ and $\%\Delta\tan\delta$ in the ZVMCD-Nb were only -1.3% and $+13\%$, respectively. The detailed variation of E_B, α, ε'_{APP}, and tan δ before and after applying the stress is summarized in Table 2.

In discussing stability, in general, macroscopically, the sintered density and the leakage current have a significant effect on the stability against stress. That is, the higher the sintered density and the lower the leakage current, the higher the stability. The low sintered density decreases the number of parallel conduction path and eventually leads to the concentration of current. The high leakage current gradually increases the carrier generation due to Joule heat and it leads to repetition cycle between joule heating and leakage current. In this viewpoint, although the high leakage current, the ZVMCD-Al did not exhibit any thermal run-away. On the contrary, although the lowest leakage current, the ZVMCD-Bi exhibited the thermal run-away. Therefore, it is difficult to assert that macroscopic factors such as sintered density and leakage current affect the stability. Microscopically, this is related to the

Table 2
E–J and dielectric characteristic parameters before and after applying the stress the samples for different dopants.

Sample	Stress state	E_B (V cm^{-1})	α	J_L (μA cm^{-2})	ε'_{APP} (1 kHz)	tan δ (1 kHz)
ZVMCD	Initial	7013	32	90	385	0.23
	Stressed	4551	5	131	627	0.82
ZVMCD-Al	Initial	2514	17	340	1555	0.26
	Stressed	2356	11	402	1531	0.28
ZVMCD-Nb	Initial	3355	36	85	775	0.31
	Stressed	3343	29	186	765	0.35
ZVMCD-Bi	Initial	4367	35	42	621	0.15
	Stressed	2815	6	534	894	0.47
ZVMCD-La	Initial	4772	12	403	631	0.5
	Stressed	3042	4	698	901	0.86

rather migration of zinc interstitial (Zn_i) within depletion layer [18]. In this viewpoint, it is guessed that the reason why the ZVMCD-Nb exhibits good stability is because the Nb spatially restricts the migration of ions within the depletion layer.

4. Conclusions

The electrical, dielectric properties, and its accelerated aging behavior of ZnO–V_2O_5–MnO_2–Co_3O_4–Dy_2O_3 (ZVMCD) ceramics were investigated with different dopants (Al, Nb, Bi, La). On one hand, Nb and Bi dopants enhanced the nonlinear coefficient whereas Al and La dopants decreased it. On the other hand, Nb and Al dopants improved the stability against aging stress. The Nb-doped ZVMCD ceramics exhibited the best nonlinear properties ($\alpha = 36$) and the highest stability: $\%\Delta E_B = -0.4\%$, $\%\Delta\alpha = -20\%$, $\%\Delta\varepsilon'_{APP} = -1.3\%$, and $\%\Delta\tan\delta = +13\%$ for DC accelerated aging stress of 0.85 E_B/85 °C/24 h.

References

[1] L.M. Levinson, H.R. Philipp, Zinc oxide varistor—a review, Am. Ceram. Soc. Bull. 65 (1986) 639–646.

[2] T.K. Gupta, Application of zinc oxide varistor, J. Am. Ceram. Soc. 73 (1990) 1817–1840.

[3] C.-W. Nahm, C.-H. Park, H.-S. Yoon, Highly stable nonohmic characteristics of ZnO–Pr_6O_{11}–CoO–Dy_2O_3 based varistors, J. Mater. Sci. Lett. 19 (2000) 725–727.

[4] C.-W. Nahm, Influence of La_2O_3 additives on microstructure and electrical properties of ZnO–Pr_6O_{11}–CoO–Cr_2O_3–La_2O_3-based varistors, Mater. Lett. 59 (2005) 2097–2100.

[5] J.-K. Tsai, T.-B. Wu, Non-ohmic characteristics of ZnO–V_2O_5 ceramics, J. Appl. Phys. 76 (1994) 4817–4822.

[6] J.-K. Tsai, T.-B. Wu, Microstructure and nonohmic properties of binary ZnO–V_2O_5 ceramics sintered at 900 °C, Mater. Lett. 26 (1996) 199–203.

[7] C.T. Kuo, C.S. Chen, I.-N. Lin, Microstructure and nonlinear properties of microwave-sintered ZnO–V_2O_5 varistors. I. Effect of V_2O_5 doping, J. Am. Ceram. Soc. 81 (1998) 2942–2948.

[8] H.-H. Hng, K.M. Knowles, Characterisation of $Zn_3(VO_4)_2$ phases in V_2O_5-doped ZnO varistors, J. Eur. Ceram. Soc. 19 (1999) 721–726.

[9] H.-H. Hng, L. Halim, Grain growth in sintered ZnO–1 mol% V_2O_5 ceramics, Mater. Lett. 57 (2003) 1411–1416.

[10] H.-H. Hng, P.L. Chan, Microstructure and current–voltage characteristics of ZnO–V_2O_5–MnO_2 varistors, Ceram. Int. 30 (2004) 1647–1653.

[11] C.-W. Nahm, Microstructure and electrical properties of vanadium-doped zinc oxide-based non-ohmic resistors, Solid State Commun. 143 (2007) 453–456.

[12] C.-W. Nahm, Improvement of electrical properties of V_2O_5 modified ZnO ceramics by Mn-doping for varistor applications, J. Mater. Sci.: Mater. Electron. 19 (2008) 1023–1029.

[13] C.-W. Nahm, Influence of Mn doping on microstructure and DC-accelerated aging behaviors of ZnO–V_2O_5-based varistors, Mater. Sci. Eng. B 150 (2008) 32–37.

[14] C.-W. Nahm, Effect of MnO_2 addition on microstructure and electrical properties of ZnO–V_2O_5-based varistor ceramics, Ceram. Int. 35 (2009) 541–546.

[15] J.C. Wurst, J.A. Nelson, Lineal intercept technique for measuring grain size in two-phase polycrystalline ceramics, J. Am. Ceram. Soc. 55 (1972) 109–111.

[16] J. Fan, R. Freer, Deep level transient spectroscopy of zinc oxide varistors doped with aluminum oxide and/or silver oxide, J. Am. Ceram. Soc. 77 (1994) 2663–2668.

[17] C.-W. Nahm, Preparation and varistor properties of new quaternary Zn–V–Mn–(La, Dy) ceramics, Ceram. Int. 35 (2009) 3435–3440.

[18] T.K. Gupta, W.G. Carlson, A grain-boundary defect model for instability/stability of a ZnO varistor, J. Mater. Sci. 20 (1985) 3487–3500.